

## Coral Reef Drag Coefficients – Water Depth Dependence

S. J. LENTZ

*Physical Oceanography, Woods Hole Oceanographic Institution, Woods Hole, Massachusetts*

K. A. DAVIS

*Department of Civil and Environmental Engineering, University of California, Irvine, Irvine, California*

J. H. CHURCHILL

*Physical Oceanography, Woods Hole Oceanographic Institution, Woods Hole, Massachusetts*

T. M. DECARLO

*Massachusetts Institute of Technology/Woods Hole Oceanographic Institution Joint Program in Oceanography and Applied Ocean Science and Engineering, Woods Hole, Massachusetts*

(Manuscript received 7 November 2016, in final form 24 February 2017)


### ABSTRACT

A major challenge in modeling the circulation over coral reefs is uncertainty in the drag coefficient because existing estimates span two orders of magnitude. Current and pressure measurements from five coral reefs are used to estimate drag coefficients based on depth-average flow, assuming a balance between the cross-reef pressure gradient and the bottom stress. At two sites wind stress is a significant term in the cross-reef momentum balance and is included in estimating the drag coefficient. For the five coral reef sites and a previous laboratory study, estimated drag coefficients increase as the water depth decreases consistent with open channel flow theory. For example, for a typical coral reef hydrodynamic roughness of 5 cm, observational estimates, and the theory indicate that the drag coefficient decreases from 0.4 in 20 cm of water to 0.005 in 10 m of water. Synthesis of results from the new field observations with estimates from previous field and laboratory studies indicate that coral reef drag coefficients range from 0.2 to 0.005 and hydrodynamic roughnesses generally range from 2 to 8 cm. While coral reef drag coefficients depend on factors such as physical roughness and surface waves, a substantial fraction of the scatter in estimates of coral reef drag coefficients is due to variations in water depth.

### 1. Introduction

The defining hydrodynamic characteristic of coral reefs is their roughness. Estimates of drag coefficients for coral reefs are typically one to two orders of magnitude larger than for sandy beaches or continental shelves (e.g., [Monismith 2007](#)). The large drag coefficients and energetic flows over shallow coral reefs result in large bottom stresses that are invariably a dominant element of the dynamics ([Roberts et al. 1975](#);

[Symonds et al. 1995](#); [Kraines et al. 1998](#); [Callaghan et al. 2006](#); [Coronado et al. 2007](#); [Jago et al. 2007](#); [Hench et al. 2008](#); [Lowe et al. 2009](#); [Vetter et al. 2010](#); [Taebi et al. 2011](#); [Monismith et al. 2013](#)). Consequently, one of the major challenges in modeling currents over coral reefs is determining accurate estimates of drag coefficients. However, drag coefficients over reefs are estimated using a wide variety of approaches and span a broad range without a clear framework for interpreting the consistency of the various estimates ([Rosman and Hench 2011](#)). As noted by [Rosman and Hench \(2011\)](#), “the broad range of reported drag coefficient values thus presents a significant challenge to predictive modeling.” They conclude their paper “we urge caution when using published  $C_D$  [drag coefficient] or  $z_0$  [hydrodynamic roughness scale] values for coral reefs.”

 Denotes content that is immediately available upon publication as open access.

Corresponding author: Steven Lentz, slentz@whoi.edu

DOI: 10.1175/JPO-D-16-0248.1

© 2017 American Meteorological Society. For information regarding reuse of this content and general copyright information, consult the [AMS Copyright Policy \(www.ametsoc.org/PUBSReuseLicenses\)](#).

Estimated drag coefficients over coral reefs are often based on the depth-average flow  $U$ :

$$\tau^b = \rho C_{da} U |U|, \quad (1)$$

where  $\tau^b$  is bottom stress,  $\rho$  is density, and  $C_{da}$  is the drag coefficient for depth-average flow (e.g., Lugo-Fernández et al. 1998a,b; Hench et al. 2008; Lowe et al. 2009; Rosman and Hench 2011; Monismith et al. 2013). Depth-average flows are often used because the traditional approach of defining a drag coefficient for the flow at a specific height above bottom is challenging over coral reefs where the precise location of the bottom is ambiguous and because the depth-average flow tends to be a more robust quantity than the velocity at a specific height. However, a consequence of using the depth-average flow to estimate bottom stress is that  $C_{da}$  depends on water depth (e.g., Nikuradse 1950; Keulegan 1938; Rouse 1965; Nezu and Nakagawa 1993). The dependence of  $C_{da}$  on water depth was included in some early studies of nutrient uptake by corals (e.g., Atkinson and Bilger 1992; Hearn et al. 2001), and a more recent laboratory study of flow over coral (McDonald et al. 2006) indicates that the drag coefficient depends on water depth. However, studies estimating the drag coefficient over coral reefs using field measurements have not generally considered the dependence of the drag coefficient on water depth [though see Pomeroy et al. (2012) and Lowe et al. (2015) for two exceptions].

This study tests two hypotheses: 1) that coral reef drag coefficients based on depth-average flow depend on water depth in a manner consistent with theory from open channel flow (reviewed in section 2) and 2) that a substantial fraction of the scatter in coral reef drag coefficients noted by Rosman and Hench (2011) is due to variations in water depth. We initially reexamine the laboratory study of McDonald et al. (2006) to determine whether the theory reproduces the water depth dependence of their drag coefficients (section 4a). We then examine drag coefficient and hydrodynamic roughness estimates (section 4b) from new observations over four coral reefs: two platform coral reefs in the Red Sea, the Palau barrier reef, and the Dongsha Atoll barrier reef (described in section 3). In section 5 we combine these new drag coefficient estimates with previous estimates from reef and laboratory studies to show that open channel flow theory provides a useful framework for characterizing the drag coefficient and hydrodynamic roughness, and that water depth variations contribute to the large scatter in drag coefficients reported by Rosman and Hench (2011). Other factors influencing drag coefficients are discussed in section 6: the Reynolds number (Re) as an indication of whether the flow is fully

turbulent (Schlichting 1968), surface gravity waves that may enhance the drag on the lower-frequency current (Hearn 1999; Monismith 2007; Lowe and Falter 2015), and the physical roughness and its relationship to estimates of hydrodynamic roughness (Monismith 2007; Hearn 2011). Key results are summarized in section 7.

## 2. Drag coefficient dependence on water depth

A dynamically based estimate of  $C_{da}$  is used from open channel flow. In turbulent open channel flow with roughness elements that are small compared to the water depth, the current profile is well represented by

$$u(\tilde{z}) = \frac{u_*}{\kappa} \left[ \log\left(\frac{\tilde{z}}{z_o}\right) + 2\Pi \sin^2\left(\frac{\pi\tilde{z}}{2D}\right) \right], \quad (2)$$

where  $u(\tilde{z})$  is the velocity profile,  $\kappa = 0.4$  is the von Kármán constant,  $u_* = \sqrt{|\tau^b|/\rho}$  is the shear velocity,  $\tilde{z}$  is the height above the bottom,  $z_o$  is the hydrodynamic roughness scale,  $\Pi$  is Cole's wake strength, and  $D$  is the water depth (e.g., Nezu and Nakagawa 1993). The first term in (2) is the classic law-of-the-wall logarithmic profile and the second term is Cole's wake function that accounts for the presence of a vertically uniform pressure gradient. For high Reynolds number open channel flow,  $\Pi \approx 0.2$  (Fig. 4.2 in Nezu and Nakagawa 1993). This value is used throughout this study. Integrating (2) from  $z = z_o$  to  $z = D$  and assuming  $z_o \ll D$ , the transport  $q$  is

$$q \approx \frac{Du_*}{\kappa} \left[ \log\left(\frac{D}{z_o}\right) + (\Pi - 1) \right]. \quad (3)$$

Dividing  $q$  by  $D$  to get the depth-average velocity  $U$  and using (1),

$$C_{da} \approx \kappa^2 \left[ \log\left(\frac{D}{z_o}\right) + (\Pi - 1) \right]^{-2}. \quad (4)$$

The key result is that  $C_{da}$  depends on the water depth  $D$  as well as  $z_o$  and  $\Pi$ . Furthermore, for high Reynolds number flows where  $\Pi \approx 0.2$ ,  $C_{da}$  from (4) only depends on the ratio  $D/z_o$ . (Other factors influencing  $C_{da}$  are discussed in section 6.) For  $D/z_o > 100$  (e.g.,  $D > 5$  m for  $z_o = 5$  cm),  $C_{da} \approx 0.01$  and is not very sensitive to variations in water depth (Fig. 1). For  $D/z_o < 50$ ,  $C_{da}$  increases rapidly as  $D/z_o$  decreases. For example, when  $D/z_o = 20$  ( $D = 1$  m for  $z_o = 5$  cm),  $C_{da} \approx 0.03$  is 3 times larger than the deep-water value. Thus, the water depth dependence of  $C_{da}$  may be important over shallow reefs (water depths of a few meters or less) where there are often relatively large temporal and spatial variations in water depth.

The applicability of (4) is based on the assumption that (2) is an accurate representation of the current

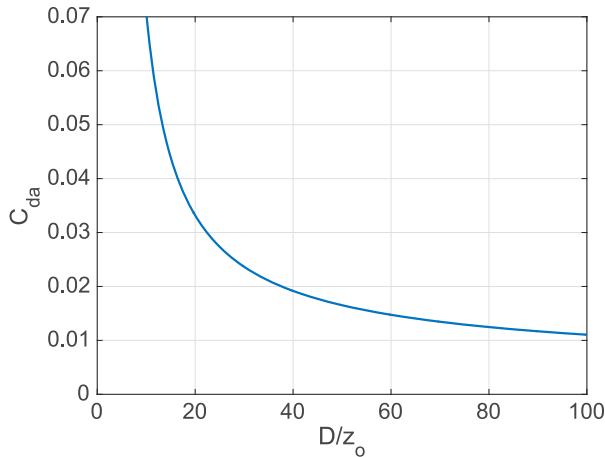


FIG. 1. The  $C_{da}$  dependence on  $D/z_o$  from (4) ( $\kappa = 0.4$  and  $\Pi = 0.2$ ).

profile over coral reefs. This implies a fully turbulent, unidirectional flow with the dominant balance between a barotropic pressure gradient and bottom stress. Thus, the water has to be shallow enough (nominally 10 m or less) and the bottom stress large enough that rotation, stratification, and other terms in the momentum balance are not important. As noted above, the water must also be deep relative to the hydrodynamic roughness  $D/z_o > 10$ , roughly  $D > 0.5$  m. Additionally, (2) may be valid above a dense canopy, but it does not describe the flow within the canopy (Rosman and Hench 2011). Thus, (4) should be valid for flows over shallow coral reefs driven by tides or wave setup (outside the surf zone). On the fore reef,  $C_{da}$  should still depend on water depth, but the relevance of (4) in the surf zone is unclear because the wave forcing (radiation stress) likely modifies the current profile (2). Furthermore, if wave-orbital velocities are large on the fore reef, the drag coefficient for the low-frequency flow will probably depend on the waves (section 6).

### 3. Overview coral reef sites, measurements, and processing

#### a. Overview of sites and instrument arrays

Drag coefficients are estimated for four shallow coral reefs spanning a variety of geometries and forcing conditions: QD3 (in Qita Dukais reef system) and Al Fahal reefs in the Red Sea, the barrier reef of Palau in the western Pacific, and Dongsha Atoll in the South China Sea (Figs. 2–5). Estimates from a previously studied fifth reef, QD2 in the Red Sea, are also included in the analyses (Lentz et al. 2016a). Instrument arrays of one or two Nortek Aquadopp current profilers bracketed by Seabird SBE26 Seagauge pressure gauges were deployed across

each reef (Figs. 2–5). Deployments were 6–12 months for the Red Sea reefs, 1–3 weeks for Palau, and 2 weeks for Dongsha (Table 1). Bathymetry was measured along each instrument transect. Details of the instrumentation, the bathymetry, wind, and surface gravity wave measurements at each site and the data processing are given in the appendix.

QD3 is a small, 250-m-long and 100-m-wide platform reef located about 10 km offshore of the Saudi Arabian coast in the central Red Sea (Fig. 2). QD3 is about 1 m deep (Fig. 2, inset) and is composed of pavement, coral rubble, small corals, and a few holes with sand (e.g., site S3; Bernstein et al. 2016). QD3 is sheltered from the prevailing wave forcing (from the northwest) by QD2 and two other small reefs. Nevertheless, the combination of forcing by winds and small waves that propagate between and around the sheltering reefs (e.g., Fig. 2) drive depth-average currents of  $5\text{--}10\text{ cm s}^{-1}$ . Significant wave heights over QD3 are typically 10 cm with orbital velocities of about  $10\text{ cm s}^{-1}$ . QD2 is about twice the size of QD3 and is exposed to incident significant wave heights that occasionally exceed 1 m with periods of about 6 s. The waves break at the front edge of the reef, causing a setup that drives peak cross-reef currents of  $\sim 20\text{ cm s}^{-1}$  (Lentz et al. 2016a). Over the QD2 reef flat, onshore of the surf zone, significant wave heights are typically 10 cm with orbital velocities of  $10\text{ cm s}^{-1}$  (Lentz et al. 2016b).

Al Fahal is a 9-km-long and 0.5–1-km-wide coral reef aligned roughly north–south and located about 12 km offshore of the Saudi Arabian coast (Fig. 3a). The water depth along the instrument transect increases from 0.6 m near the front edge of the reef to 3 m near the back edge (Fig. 3c). The seaward half of the reef is composed of pavement, coral rubble, small corals, and narrow channels (A2–A3). The shoreward half of the reef is sand (light regions between A4 and A5 in Fig. 3b) with a broken line of shallow platform reefs running north–south along the back edge of the reef (A6). Depth-average cross-reef currents are typically  $10\text{--}20\text{ cm s}^{-1}$  (at A3) and are driven by incident surface gravity waves with wave heights of 1–2 m and peak periods of about 6 s. Significant wave heights onshore of the surf zone over Al Fahal are typically 7–8 cm with orbital velocities of about  $5\text{ cm s}^{-1}$ .

Palau's main island and complex system of connected lagoons are surrounded by a barrier reef (Fig. 4a) that is  $\sim 1.2$  km wide at the instrument transects (Fig. 4b). The mean water depth increases from 1 m near the seaward edge of the reef to 3 m at the edge of the large lagoon (Fig. 4c). Near the reef crest (P1) the bottom is primarily small corals and rubble, transitioning to a mix of sand and coral (P2) and primarily sand with intermittent small patch reefs over the back half of the barrier reef (P3 to the lagoon; Barkley et al. 2015). Depth-average

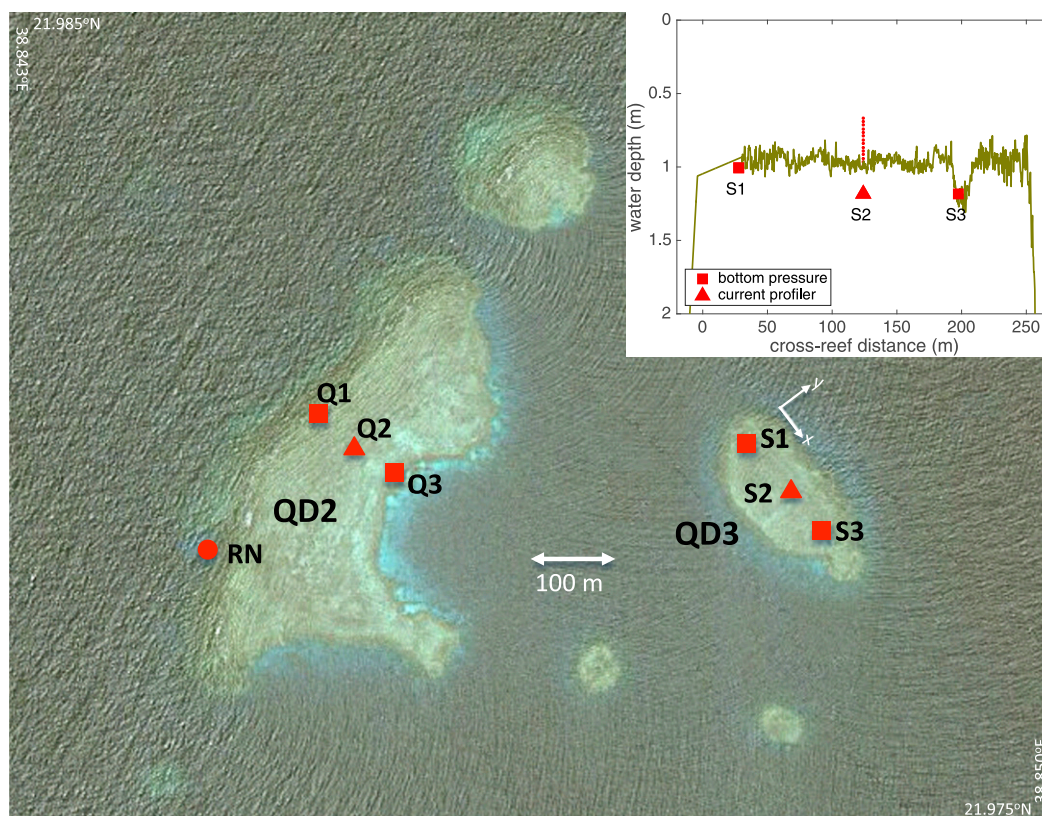


FIG. 2. Satellite image (Apple Maps) of Red Sea platform reefs QD2 and QD3 in the Qita Dukais reef system and pressure gauge (squares) and current profiler (triangles) locations. QD3 is sheltered from surface waves that typically propagate southeastward. Incident surface wave measurements were made at location RN. Inset shows bathymetry and instrument locations along QD3 transect. The current profiler at S2 was in a small hole (similar to S3) that was slightly off the bathymetry transect.

cross-reef currents are primarily tidal with peak speeds of  $30\text{--}40\text{ cm s}^{-1}$  (at P3) during spring tides. Significant wave heights over the Palau barrier reef are modulated by the tide (larger waves during higher tides) and range from 15 cm near the reef crest to 5 cm over the back half of the reef. Corresponding wave orbital velocities range from  $25\text{ cm s}^{-1}$  near the reef crest to  $5\text{ cm s}^{-1}$  over the back half of the reef. Incident wave characteristics were not measured.

Dongsha Atoll is a circular coral reef in the South China Sea near the shelf break, about 300 km offshore of China. Dongsha is about 20 km in diameter with a central lagoon surrounded by a 3-km-wide barrier reef (Fig. 5a). Mean water depth along the instrument transect on the eastern side of the reef (Fig. 5b) increases across the barrier reef from 0.6 m over the seaward side to 2.5 m at the lagoon edge (Fig. 5c). The barrier reef included rubble and small (typically 20–30 cm) corals and seagrass patches between E2 and E4, and sand, seagrass, massive *Porites* colonies and *Acropora* thickets (both commonly  $>1\text{ m}$  height) between E4 and E6

(DeCarlo et al. 2017). Depth-average cross-reef currents of  $10\text{--}30\text{ cm s}^{-1}$  (at E5) are forced by tides and surface gravity waves. Incident significant wave heights were less than 0.5 m during the first half of the deployment, then exceeded 1 m for 6 days, reaching a peak height of 3 m. Peak periods were typically 10 s. Over the reef, wave heights are modulated by the tide. On the lagoon side of the surf zone, wave heights were typically 10 cm near the crest, with occasional peaks exceeding 0.5 m during high tides when the incident waves were largest. Orbital velocities at the crest were typically  $10\text{ cm s}^{-1}$  with peaks exceeding  $50\text{ cm s}^{-1}$ . At midreef, wave heights and orbital velocities were undetectable, less than a few centimeters or centimeters per second, respectively.

#### *b. Cross-reef momentum balance and estimation of drag coefficient*

Drag coefficients and hydrodynamic roughnesses are estimated using the pressure and current profile measurements following the procedure in Lentz et al. (2016a).



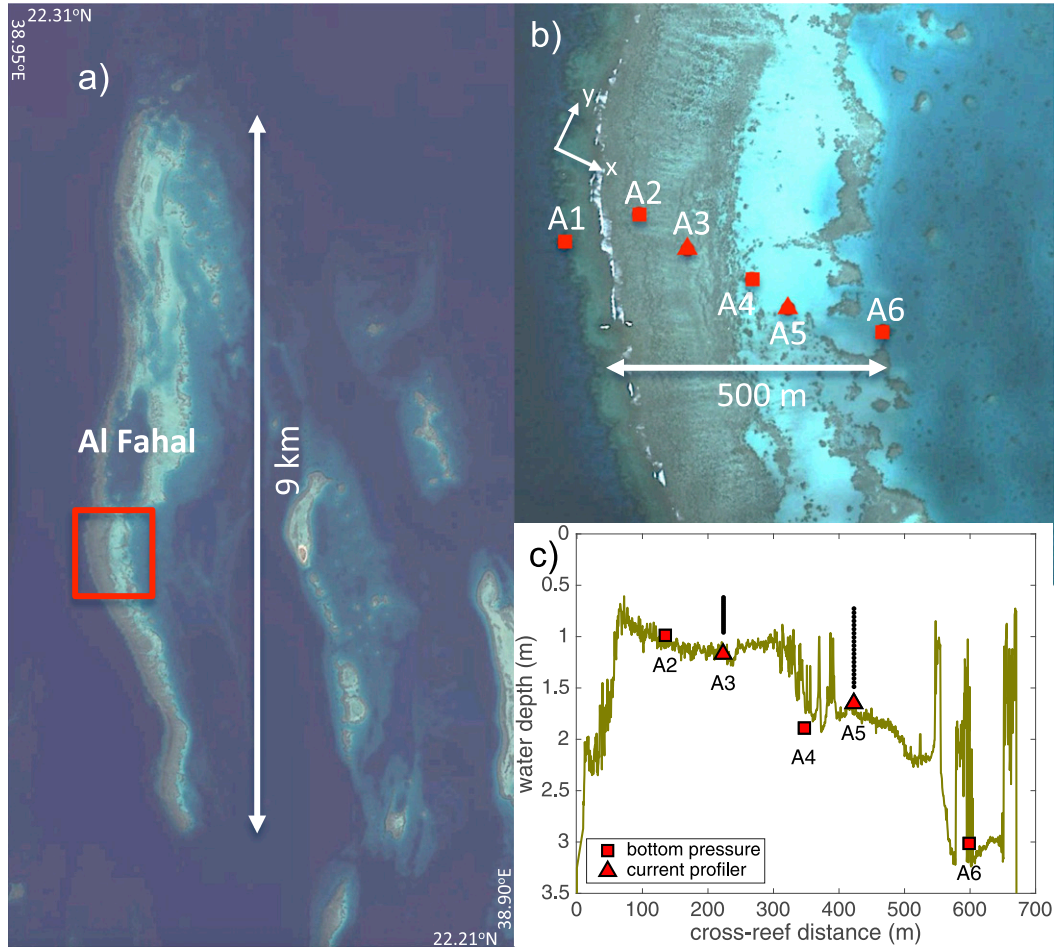


FIG. 3. Satellite image (Google Earth) of (a) Al Fahal reef in the Red Sea, (b) the pressure gauge (squares) and current profiler (triangles) locations, and (c) bathymetry and instrument locations across the reef.

Briefly, assuming cross-reef transport is conserved,  $U(x, t)D(x, t) = q_o(t)$ , and that the cross-reef pressure gradient is balanced by the wind stress and bottom stress over the reef flat (all sites are outside the surf zone),

$$gD \frac{\partial \eta}{\partial x} = \frac{\tau^{sx}}{\rho} - \frac{\tau^{bx}}{\rho} \quad \text{where} \quad \frac{\tau^{bx}}{\rho} = C_{da} U|U| = C_{da} \frac{q_o |q_o|}{D^2}, \quad (5)$$

where  $g$  is gravitational acceleration,  $\eta$  is the sea surface variation, and  $\tau^{sx}$  and  $\tau^{bx}$  are the cross-reef components of the wind stress and bottom stress. Assuming sea level variations on the scale of the reef are small compared to the water depth ( $\eta \ll D$ ), dividing (5) by  $D$ , and integrating across the reef between pressure measurements at  $x_1$  and  $x_2$  yields

$$g\Delta\eta = \int_{x_1}^{x_2} (\tau^{sx}/\rho) D^{-1} dx - C_B q_o |q_o| \int_{x_1}^{x_2} D^{-3} dx, \quad (6)$$

where  $\Delta\eta = \eta(x_2) - \eta(x_1)$ ,  $C_{da}$  is given by (4), and

$$C_B = \frac{\int_{x_1}^{x_2} C_{da} D^{-3} dx}{\int_{x_1}^{x_2} D^{-3} dx}. \quad (7)$$

A simple finite difference estimate of (5) between two pressure measurement sites is inaccurate if the cross-reef bathymetry varies because of the nonlinear dependence on water depth  $D$ . The sea surface is curved because the flow in shallower water is larger to conserve transport and consequently the bottom stress and hence the sea surface slope is larger in shallow water than in deep water. Wind stress is estimated following Fairall et al. (2003) (see appendix for details). The wind stress term in (5) or (6) is negligible in all but two cases, QD3 in the Red Sea and the lagoon side of the Dongsha barrier reef [section 4b(2)].

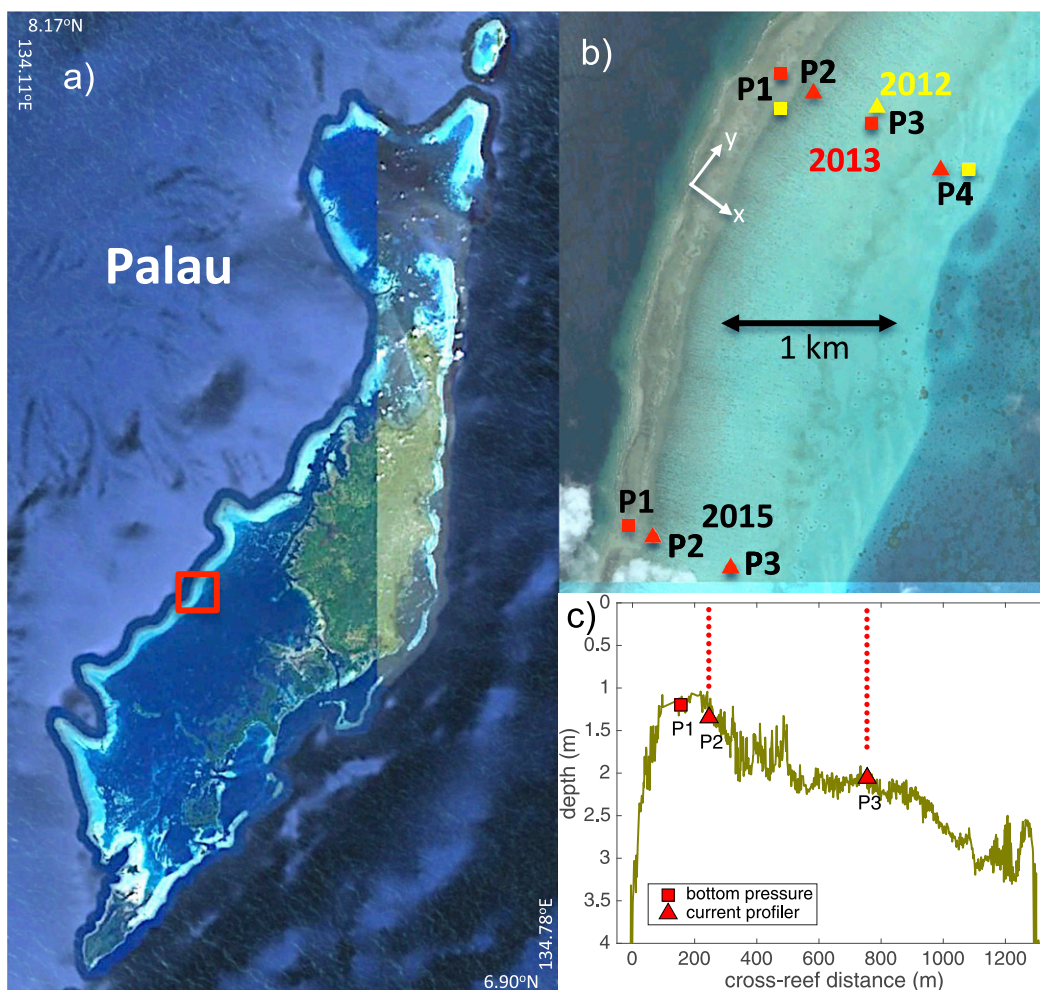


FIG. 4. Satellite image (Google Earth) of (a) Palau main island and reef system; (b) the western barrier reef with the pressure gauge (squares) and current profiler (triangles) locations for the 2012, 2013, and 2015 deployments; and (c) bathymetry and instrument locations across the barrier reef at the 2015 instrument transect. Bathymetry along 2012–13 transect is similar.

The terms in (6) are estimated using time series of sea level from the pressure gauges, cross-reef transports from the current profilers, wind stress, and water depth determined from the bathymetry transects and the sea level time series. For each site during each deployment a single value of  $z_o$  is determined that minimizes the root-mean-square (RMS) difference between the left- and right-hand sides of (6) with  $C_{da}$  estimated from (4) (Table 1).

#### 4. Results

##### a. Laboratory

In a set of laboratory experiments with coral heads (*Porites compressa*) covering the bottom of a 10-m-long, 0.6-m-wide flume, McDonald et al. (2006) found that  $C_{da}$  depended on water depth. The sequence of experiments

included varying the water depth  $D$  from 0.2 to 0.4 m and the speed of a unidirectional flow from 3 to 36  $\text{cm s}^{-1}$ . The drag coefficient was estimated as  $C_{da} = gD(\partial\eta/\partial x)/U^2$ , where  $\partial\eta/\partial x$  is the along-flume surface slope [the factor of 2 in the numerator of the McDonald et al. expression is not included here to be consistent with the definition of  $C_{da}$  in (1)]. McDonald et al. found that a power law with three empirical constants  $C_{da} = 1.01(D/h_c)^{-2.77} + 0.01$  accurately represented the relationship between the drag coefficient and the ratio of the water depth to the maximum coral height ( $h_c = 0.18$  m) for the runs with maximum Reynolds number at each water depth (Fig. 6, solid line). McDonald et al.'s empirical relationship is consistent with power laws proposed for rivers (e.g., Smart et al. 2002), though with different coefficients. Rosman and Hench (2011) note that while these results indicate a

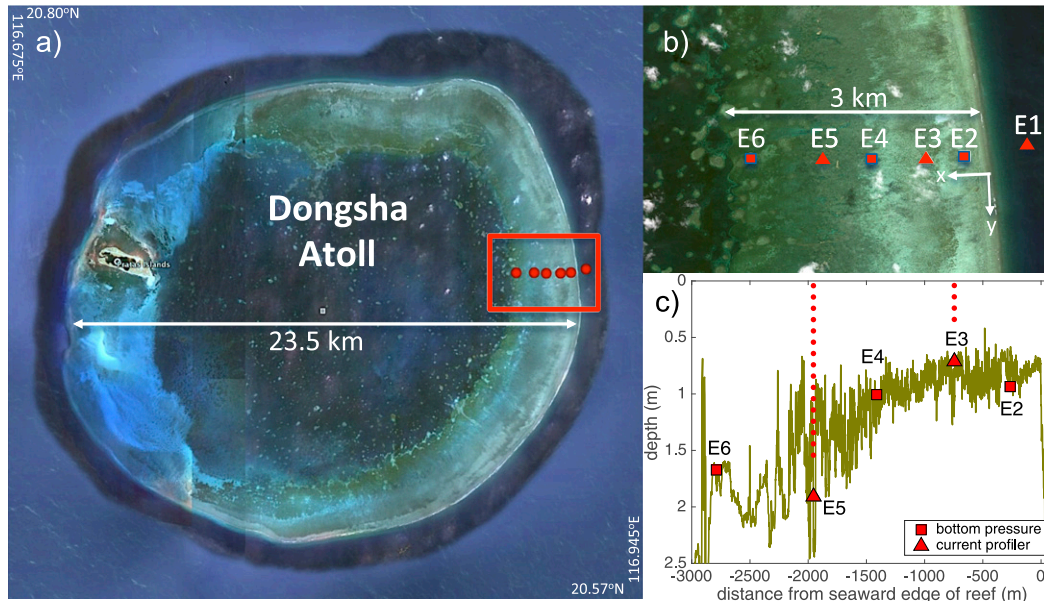


FIG. 5. Satellite image (Google Earth) of (a) Dongsha Atoll in the South China Sea, (b) the eastern portion of the barrier reef with pressure gauge (squares) and current profiler (triangles) locations, and (c) bathymetry and instrument locations across Dongsha's barrier reef at the instrument transect.

dependence of  $C_{da}$  on water depth, it is unclear how to extend this empirical relationship to other laboratory or field studies without a physical interpretation of the three coefficients. Equation (4) also accurately reproduces McDonald et al.'s drag coefficient estimates with a single empirical constant  $z_o = 4.6$  cm (Fig. 6, dashed line). Neither McDonald et al.'s empirical relationship or (4) accurately estimate the large values of  $C_{da}$  at the shallowest water depth (0.2 m). McDonald et al. (2006) note that these runs were low Reynolds

number flows that may have been in a transitional regime between laminar and fully turbulent flow. These laboratory runs are also at small values of  $D/h_c$  (Asher et al. 2016).

### b. Coral reefs

#### 1) CROSS-REEF TRANSPORTS

The momentum balance analysis to estimate drag coefficients assumes that cross-reef transport is conserved

TABLE 1. Summary of study site features and analyses including the McDonald et al. (2006) laboratory experiments. Variable  $D$  is the depth range at each site,  $\Delta\eta_{std}$  is the standard deviation of the cross-reef sea level difference,  $U_{std}$  is the standard deviation of the depth-average cross-reef current, and  $z_o$  is the hydrodynamic roughness estimate. The last two columns show the minimum RMS difference and the correlation between terms in (6). Correlations are all significant at the 95% confidence level. Estimates of  $z_o$ , RMS difference, and correlations in parentheses for QD3 and Dongsha E4–E6 include wind stress in (6).

Study site reef type	Instr. sites	Bottom type	Length (days)	$D$ (m)	$\Delta\eta_{std}$ (cm)	$U_{std}$ (cm s <sup>-1</sup> )	$z_o$ (cm)	RMS (cm)	Corr.
Laboratory		Coral	—	0.2–0.4	0.8	—	4.6	0.2	0.95
QD2 platform	Q1–Q3	Pavement, small corals	357	0.4–1.3	1.1	5	6.0	0.3	0.97
QD3 platform	S1–S3	Pavement, small corals	155	0.6–1.5	0.3	2.5	5.5 (6.7)	0.2 (0.2)	0.71 (0.78)
Al Fahal platform	A2–A4	Pavement, small corals	106 <sup>a</sup>	0.4–1.5	1.7	6	5.3	0.5	0.96
	A4–A6	Sand, small reefs	157	1.3–2.4	0.4	6	5.8	0.2	0.85
Palau 2012 barrier	P1–P4	Rubble, corals, sand	5	1.2–3.2	1.7	11	7.5	0.5	0.95
Palau 2013 barrier	P1–P3	Rubble, corals, sand	4.5	0.7–2.8	2.5	15	6.7	0.5	0.98
	P3–P4	Sand	4.5	1.3–3.4	0.3	9	2.8	0.2	0.91
Palau 2015 barrier	P1–P2	Rubble, corals,	18 <sup>a</sup>	0.5–2.1	4.7	23	6.3	1.5	0.93
	P2–P3	Sand	25	1.3–2.8	2.9	12	6.3	1.1	0.92
Dongsha Atoll	E2–E4	Rubble, corals seagrass	7 <sup>a</sup>	0.2–1.7	7.2	16	3.2	1.6	0.96
	E4–E6	Sand, seagrass large corals	13	0.9–2.4	1.2	6	1.4 (1.7)	1.0 (0.8)	0.75 (0.87)

<sup>a</sup> There are fewer observations at sites near the seaward edge of the reef because the water was often too shallow to obtain current profiles.



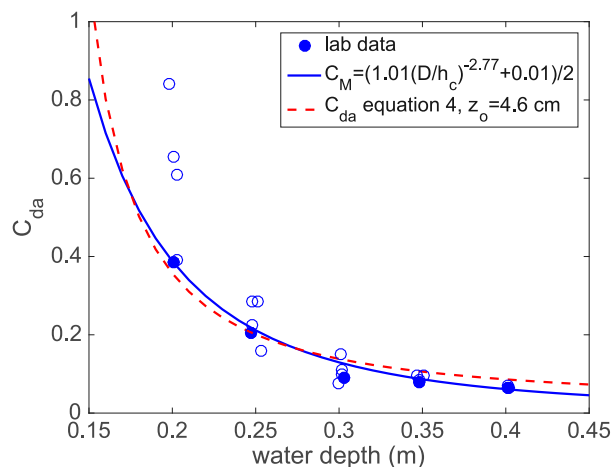


FIG. 6. Estimates of the drag coefficient as a function of water depth for the laboratory experiments of McDonald et al. (2006). Solid circles are experiments with highest Re at each water depth. The empirical fit of McDonald et al. for the highest Re experiments and the fit to (4) are also shown.

across the reef. This assumption was tested for deployments that included two current profilers (Al Fahal, Dongsha Atoll, and Palau 2013 and 2015; Figs. 3–5). Correlations between the cross-reef transport time series from the two profilers range from 0.95 to 0.99 (significantly larger than zero at the 99% confidence level). However, regression slopes indicate marginally significant (11%–18%) differences in transport magnitude for three of the four sites.

Over Al Fahal the A3 transport is  $0.71 \pm 0.18$  (95% confidence interval) times the A5 transport. The larger transport at A5 is probably due to the line of shallow platform reefs along the back edge of Al Fahal that reduce the cross-sectional area and force enhanced transport through the gaps, including the gap near A5 and A6 (Fig. 3b).

At the northern (2013) transect on the Palau barrier reef, transports at P2 and P4 are within 1% of each other. At the southern (2015) transect the P2 transport is  $1.16 \pm 0.13$  times the P3 transport. The cause of the transport difference is unclear, but it may be associated with variations in bathymetry along the crest at P1 and P2 (Fig. 4b).

At Dongsha, the E5 transport is  $1.12 \pm 0.04$  times the E3 transport. This discrepancy is not surprising, since the barrier reef is circular and consequently the transport should increase toward the center of the atoll (if the flow is radially symmetric). Based on the radial distances from the atoll center, the cross-reef transport should be 11% larger at E5 than at E3, which agrees well with the observed difference of 12%. Accounting for the radial dependence of the transport in (6) does

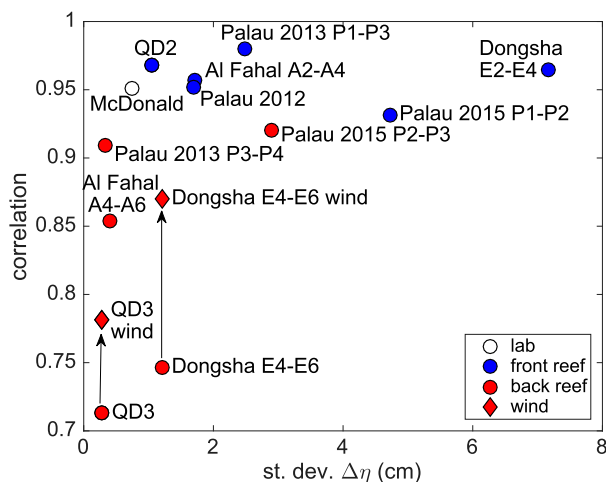


FIG. 7. Correlations between pressure difference and bottom stress terms in (6) vs standard deviation of the sea level difference for each site and the laboratory study. Sites on front half of reef or exposed are shown in blue and on the back half or protected in red. Inclusion of wind stress forcing in (6) increased correlations for QD3 and Dongsha E4–E6. Correlations are all significantly different from zero at the 95% confidence level.

not change the estimated drag coefficients or hydrodynamic roughness.

## 2) MOMENTUM BALANCES

Correlations between the pressure difference and bottom stress terms in (6) range from 0.70 to 0.98 (Fig. 7, Table 1), all significantly different from zero at the 95% confidence level. Correlations exceed 0.93 on the seaward side of all exposed reefs (blue circles Fig. 7). Correlations are lower on the lagoon or shoreward side of reefs and the sheltered reef (red circles Fig. 7), which also tend to have smaller standard deviations of cross-reef pressure differences than the seaward side of the reefs. The high correlations support the assumed balance between the cross-reef pressure gradient and the bottom stress. Direct estimates of the other terms in the cross-reef momentum balance (following Lentz et al. 2016a) are an order of magnitude smaller than the pressure difference, with two exceptions in which the cross-reef wind stress is significant. At QD3, the sheltered reef in the Red Sea where the wave forcing is weak (based on visual observations) and sea level differences are small, the wind stress term is significant. Adding the wind stress term in (6) to the pressure difference improves the correlation with the bottom stress (Fig. 7). Including the wind stress also significantly improves the momentum balance correlation on the lagoon side of Dongsha Atoll (E4–E6).

Choosing the optimal  $z_o$  results in regression slopes between the forcing terms (pressure difference plus



wind stress in two cases) and bottom stress that are within a few percent of 1. Assuming the sea surface was flat when the depth-average current speed was small ( $<2 \text{ cm s}^{-1}$ ) results in intercepts near zero (sea level differences less than 3 mm). RMS differences between the forcing terms and the bottom stress term (divided by  $g$ ) range from 0.2 to 1.6 cm and tend to increase with increasing signal (standard deviation of  $\Delta\eta$ ; Table 1). For Red Sea reefs where the more accurate pulse-coherent Doppler current profiler was used, RMS differences are generally near 0.2 cm, the presumed accuracy of the pressure measurements. At the other sites, the noisier current measurements probably make a substantial contribution to the RMS differences. These results suggest discrepancies between the forcing and bottom stress terms are primarily due to uncertainties in the estimation of these terms, rather than neglected terms in the momentum balance.

### 3) DRAG COEFFICIENT DEPENDENCE ON WATER DEPTH

If a constant drag coefficient is used instead of (4), correlations between the pressure difference and bottom stress terms are lower and the ratio of the two terms clearly depends on water depth. To explicitly test the hypothesis that the drag coefficient depends on water depth, the spatial-average (bulk) drag coefficient between pressure gauge sites was estimated directly from the terms in the momentum balance [(6)] for each sample period as

$$C_B = -g\Delta\eta / \left( q_o |q_o| \int D^{-3} dx \right) \quad (8)$$

(neglecting wind stress for simplicity; Fig. 8, circles). At every site there is a general tendency for the bulk drag coefficient to increase as the water depth decreases. Furthermore, the increase in  $C_B$  as the water depth decreases is consistent with the theoretical dependence given by (7) and (4), where  $C_B$  only depends on  $D(x, t)$  and  $z_o$  (Fig. 8, red lines). Pomeroy et al. (2012) found essentially the same dependence on water depth for drag coefficients associated with infragravity wave motions over a coral reef (Fig. 8b in their paper).

The tendency for  $C_B$  to increase slightly for water depths greater than 1 m over Al Fahal (Fig. 8a) may be related to surface gravity wave enhancement of the drag (see section 6). Over shallow reefs, the variations in  $C_B$  due to changes in water depth can be substantial. For example, near the reef crest on Palau's barrier reef  $C_B$  varies from 0.09 when the water is 0.6 m deep to 0.03 when the water is 2 m deep (Fig. 8b). These results indicate that the drag coefficient depends on water depth

and the dependence is consistent with theory based on open channel flow.

### 4) HYDRODYNAMIC ROUGHNESS $z_o$

The bulk  $z_o$  estimates from (4) and (6) range from 1.4 to 7.5 cm (Table 1). Most of the  $z_o$  estimates for the Red Sea and Palau reefs fall in a narrower range between 5.3 and 7.5 cm. The smaller values of  $z_o$  ( $\leq 3.2$  cm) are from the sandy region on the lagoon side of the Palau barrier reef (P3–P4 2013; Fig. 4) and from Dongsha Atoll. It is noteworthy that the  $z_o = 4.6$  cm estimated for the laboratory study of McDonald et al. (2006) using real corals is similar to the coral reef field estimates.

## 5. Synthesis and comparison to previous studies

The dependence of the drag coefficient  $C_{da}$  estimates on water depth from this study and previous studies is summarized in Fig. 9. For the sites examined here (red symbols Fig. 9),  $C_{da}$  is calculated from (4) using the observed range of water depths and the estimates of  $z_o$  for each site (Table 1). Most of the drag coefficient estimates from previous studies are also based on assuming a balance between the pressure gradient and bottom stress. However, the previous estimates generally use a finite difference to estimate the pressure gradient rather than integrating (5), so they may be inaccurate if the water depth varies between the pressure measurement sites. The number of samples used to estimate the drag coefficient also varies in these studies. Baird et al. (2004) use average current and pressure difference measurements over Warraber Island reef for short periods on two successive days to determine  $C_{da}$ . The Coronado et al. (2007) estimate is based on a sea level difference measurement across Puerto Morelos reef during Hurricane Ivan, assuming a maximum current of  $1 \text{ m s}^{-1}$ . Vetter et al. (2010) note that their time series measurements over Guam's fringing reef were too noisy to estimate the drag coefficient from a regression analysis, but they argued that  $C_{da} \sim 0.006$  gave reasonable agreement between terms in the momentum balance during a tropical storm. Lowe et al. (2009) use a linear regression between the pressure gradient and the bottom stress over 167 days and assume a constant water depth to estimate the drag coefficient over Kaneohe Bay reef. Rosman and Hench (2011) and Monismith et al. (2013) also use a linear regression between the pressure gradient and the bottom stress, and a time varying water depth, to estimate the drag coefficient across Moorea's back reef from time series lasting a couple months.

In contrast to the momentum balance approach, Reidenbach et al. (2006) use profile and turbulence measurements to estimate  $C_d$  and  $z_o$  at two reef sites and

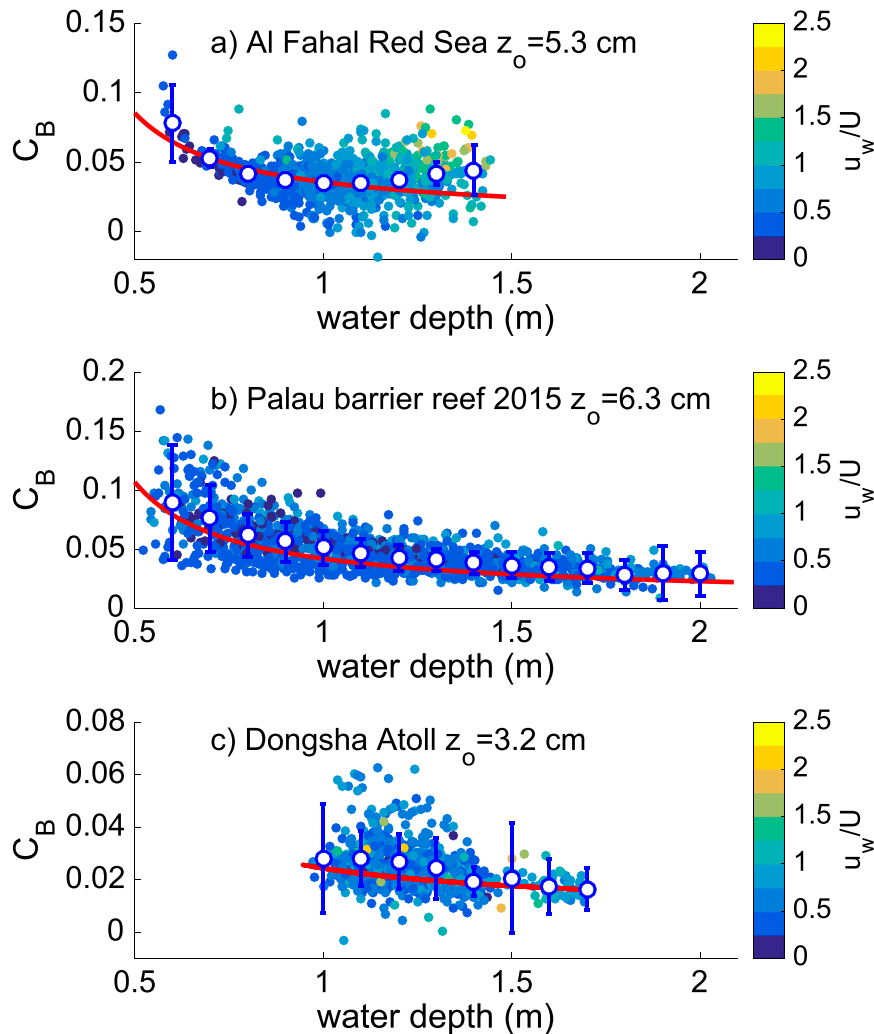


FIG. 8. Examples of bulk drag coefficient  $C_B$  dependence on water depth from observations using (8) (circles) for (a) Al Fahal, (b) Palau, and (c) Dongsha reef. Color indicates the ratio of the wave-orbital velocity  $u_w$  to the magnitude of the depth-average current. Open circles are  $C_B$  averaged over 0.1-m water-depth bin with standard error of the means indicated by error bars. Red lines are theoretical estimates from (7), using (4) and the estimates of  $z_o$  (Table 1) for each site.

one sand site in the Gulf of Aqaba in the Red Sea. Their results are compelling as they show close agreement between covariance stress, dissipation, and log-profile estimates of  $C_d$  at each site. They also observe some dependence on flow direction at each site. (Their drag coefficient estimates are for a height of 1 m above the bottom and consequently are adjusted to depth-average values assuming a log profile.) Their estimates of average  $z_o$ , 1–3.9 cm for the reef sites and 0.1–0.4 cm for the sand site, are consistent with the inferred values of  $z_o$  from Fig. 9 (squares, water depth  $\sim 10$  m). The relatively small  $C_d$  and  $z_o$  values from the sand site in the Gulf of Aqaba are consistent with estimates from shelves and beaches (e.g., Grant and Madsen 1986; Feddersen et al. 2003).

The drag coefficients summarized in Fig. 9 span almost two orders of magnitude ( $\sim 0.005$ – $0.4$ ), as previously noted by Rosman and Hench (2011). However, a substantial fraction of the variation in drag coefficients is due to variations in water depth, both spatial (different sites) and temporal (variations at sites examined in this study). Inferred hydrodynamic roughnesses  $z_o$ , are between 2 cm and 8 cm for most of the coral reef sites summarized in Fig. 9. It is notable that in this framework the  $z_o$  values inferred from turbulence estimates (Reidenbach et al. 2006) and laboratory studies (McDonald et al. 2006; Asher et al. 2016) are consistent with most of the field estimates of  $z_o$  based on momentum balances. Log-profile estimates for 10 sites on

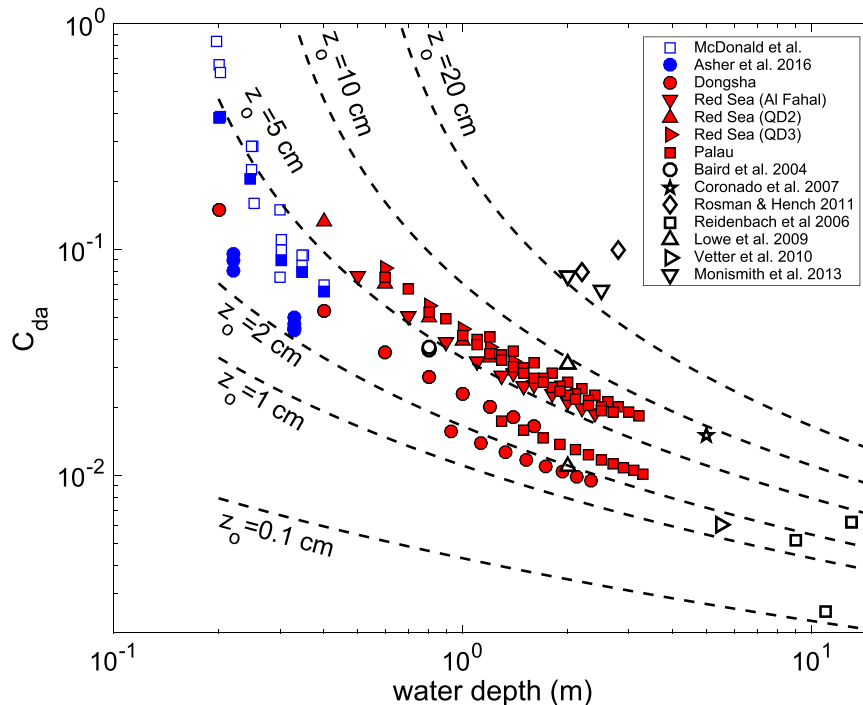


FIG. 9. Summary of the dependence of depth-average drag coefficient estimates  $C_{da}$  on water depth from laboratory studies (blue symbols), the field observations presented here (red symbols), and previous estimates for various locations (open symbols). Lines of constant  $z_o$  based on (4) are also shown. Note that  $C_{da}$  varies by two orders of magnitude but most estimates of  $z_o$  are between 2 and 8 cm, with the notable exception of four estimates from Moorea (Rosman and Hench 2011; Monismith et al. 2013), where  $z_o > 20$  cm.

Palmyra reef span a similar range of  $z_o$ , 2.2–5.5 cm (Rogers et al. 2016). For the two studies over Moorea’s back reef (Rosman and Hench 2011; Monismith et al. 2013), the inferred  $z_o$  exceeds 20 cm. The large values of  $z_o$  may be associated “with large coral bommies” that occupy a substantial fraction of the water column on the Moorea back reef (Rosman and Hench 2011).

## 6. Discussion

The results of this study emphasize the importance of accurately reproducing water depth variations in modeling studies of coral reefs. Understanding the dependence of coral reef drag coefficients on water depth is critical for properly representing drag coefficients or hydrodynamic roughnesses in models of coral reefs. It also provides a crucial framework for addressing three unresolved problems relating to drag over coral reefs: the dependence of coral reef drag coefficients on  $Re$ , the impact of surface gravity waves on drag, and the relationship between physical roughness and hydrodynamic roughness.

Coral reefs are hydrodynamically rough ( $u_* h_c / \nu > 70$ , where  $\nu$  is kinematic viscosity), even for weak currents

( $\sim 1 \text{ cm s}^{-1}$ ), suggesting the drag coefficient should be independent of the Reynolds number ( $Re = UD/\nu$ ), provided the flow is fully turbulent (Schlichting 1968). For the estimates of  $C_B$  at the different field study sites,  $Re$  ranged from  $3 \times 10^4$  to  $3 \times 10^6$ . After accounting for the dependence of  $C_B$  on  $D/z_o$ , estimates of  $C_B$  are independent of  $Re$  over that range, suggesting the flow was fully turbulent. McDonald et al. (2006) noted a dependence of  $C_{da}$  on  $Re$  at constant water depth for  $Re < \sim 3 \times 10^4$  and suggested this might be associated with a transition to turbulent flow. Accurately resolving the transition to turbulence over shallow coral reefs is challenging because the associated currents are likely to be weak, for example, a current of  $1 \text{ cm s}^{-1}$  in 1 m of water for  $Re \approx 10^4$ .

This study does not consider the influence of surface gravity waves, which should enhance the drag on the “mean” flow (time scales longer than the waves) over coral reefs. The relationship between waves and drag over coral reefs is unresolved. Existing theories on wave–current interactions (e.g., Grant and Madsen 1986) are formally not valid over coral reefs if the hydrodynamic roughness is larger than the wave boundary layer thickness. Nevertheless, the contribution of the



waves to the drag on the “mean” current probably depends on the vertical scale of the wave-driven stresses relative to the water depth. If the wave-driven turbulent stresses extend throughout the water column, then including the total flow, waves plus mean current, in the quadratic drag law may be appropriate (i.e., Feddersen et al. 2000).

The sites examined here are on reef flats behind the surf zone, and consequently for the estimated drag coefficients, the ratio of wave orbital velocity to the magnitude of the burst-average current is 2.5 or less (Fig. 8, colored circles). This is probably not the case on fore reefs and in the surf zone where wave orbital velocities may be much larger than mean flows. The fraction of surface gravity wave energy that propagates onto reefs increases as the water depth increases because of the tendency for the wave height to be proportional to the water depth in the surf zone (e.g., Raubenheimer et al. 2001; Lowe et al. 2009; Becker et al. 2014; Lentz et al. 2016b). Thus, surface waves should enhance the drag coefficient more when the water is deeper—the opposite of the dependence in (4) (Fig. 1). The Al Fahal observations appear to support this idea, waves tend to be larger when the water is deeper, and there is a tendency for enhanced drag coefficients during larger waves (Fig. 8a, colored circles). However, for the Palau barrier reef and Dongsha Atoll (Figs. 8b,c), there is not an obvious dependence of the drag coefficient on the ratio of the wave orbital velocity to the burst-average current. Lentz et al. (2016a) for QD2 and Monismith et al. (2013) for the fore reef of Moorea both found that the drag coefficient did not show any particular dependence on wave height. Clearly, the influence of waves on drag over coral reefs remains an important unresolved problem and is the subject of ongoing research using the observations in this study.

Relating hydrodynamic roughness to physical roughness over coral reefs is an important but very challenging problem (e.g., Monismith 2007; Hearn 2011). Previous studies in a variety of fields suggest the relationship between hydrodynamic and physical roughness is complex, depending, for example, on the ratio of roughness frontal area to bed area (e.g., Raupach et al. 1991; Britter and Hanna 2003; Jimenez 2004; see also Monismith et al. 2015). Consequently, determining a useful characterization of the physical roughness over coral reefs that is relevant to bottom stress is a major challenge (Nunes and Pawlak 2008; Zawada et al. 2010; Rosman and Hench 2011, Jaramillo and Pawlak 2011; Hearn 2011). Accounting for the water depth dependence of the drag coefficients to get accurate estimates of hydrodynamic roughness is an important first step. Clearly, it would be difficult to associate the drag coefficients summarized in

Fig. 9 to the physical roughness at the different coral reef sites without first accounting for the water depth variations. It is encouraging that  $z_o$  determined from the laboratory studies using real coral heads (McDonald et al. 2006; Asher et al. 2016) are typical of the field estimates, sandy regions like the Palau back reef have relatively small  $z_o$ , and the exceptionally rough Moorea back reef has large  $z_o$ .

## 7. Summary

Observations from five coral reefs spanning a range of locations, geometries, and dominant forcing and from a laboratory study (McDonald et al. 2006) indicate that the drag coefficient based on the depth-average current depends on the water depth in a manner consistent with theory from open channel flow [(4)] (Figs. 7–9). Consequently, drag coefficients vary on tidal and longer time scales due to variations in water depth over shallow coral reefs. A substantial fraction of the variation in drag coefficients over coral reefs noted by Rosman and Hench (2011) is due to variations in water depth between sites (Fig. 9).

*Acknowledgments.* The authors thank Anne Cohen—the successful Palau and Dongsha field programs are a direct consequence of her vision and leadership. We also thank Falk Feddersen and an anonymous reviewer for their constructive suggestions that substantially improved this paper.

The authors thank Dr. Yasser Abualnaja, Dr. Abdulaziz Al-Suwailem, Haitham Aljahdali, Mohsen Aljahdali, Ramzi Aljahdali, Wael Almoazen, Captain Evangelos G. Aravantinos, Yasser Kattan, the whaler crew from King Abdullah University of Sciences and Technology (KAUST), and C. Marquette of Woods Hole Oceanographic Institution (WHOI) for providing logistical and field support. The Red Sea field program was supported by Awards USA 00002 and KSA 00011 made by KAUST to S. Lentz and J. Churchill. Data are available from corresponding author (slentz@whoi.edu) upon request, subject to approval from KAUST.

The authors thank George P. Lohmann, Kathryn A. Rose, Rebecca Belastock (all WHOI), Jay Andrew, Geory Mereb, Arius Merep, Dawnette Olsudong (all PICRC), Rodney Salm, and Elizabeth Mcleod (The Nature Conservancy). The Palau field program was funded by NSF Award OCE-1220529.

We thank Keryea Soong and the Dongsha Atoll Research Station; the Dongsha Atoll Marine National Park; the crew of the Ocean Researcher 3; Pat Lohmann (WHOI); Kathryn Shamberger (Texas A&M University); Aryan Safie (UC Irvine); and Lisa Hou, Kuo-Yuan

Lee, and Yao-Chu Wu (Academia Sinica) for assistance with fieldwork and logistics. The Dongsha field program was supported by NSF Award OCE-1220529 and by the Academia Sinica (Taiwan) through a thematic project grant to George Wong and Fuh-Kwo Shiah. CCMP Version-2.0 vector wind analyses are produced by Remote Sensing Systems. Data are available at [www.remss.com](http://www.remss.com). S. Lentz was supported for the analysis by NSF Award OCE-1558343.

## APPENDIX

### Instrumentation, Sampling, and Initial Processing

The Aquadopp current profilers deployed on the Red Sea reefs burst sampled for 256 s or 300 s every hour with 2–4-cm vertical bins. They were in pulse coherent mode, providing relatively accurate current measurements (error velocity a few millimeters per second) that spanned only the lower half of the water column [see appendix in [Lentz et al. \(2016a\)](#) for processing details]. Aquadopps deployed on the Palau and Dongsha reefs burst sampled for 60 s every 4 min with 10-cm vertical bins. They were in standard mode and consequently the current profiles spanned most of the water column but were less accurate (a few centimeters per second) than the pulse coherent mode. In both cases, depth-average currents were estimated by extrapolating the velocity measurements to the surface and bottom using an empirical orthogonal function (EOF) analysis of current profiles fit to a logarithmic profile [see [Lentz et al. \(2016a\)](#) for details]. The EOF typically accounted for 95% or more of the total current variance. In all cases, results were similar using a simple vertical average of the current profile measurements. Cross-reef transport (oriented along the pressure array) was estimated by multiplying the depth-average current by the time-varying water depth.

The Seagauges recorded mean pressures, from a continuously sampled Paroscientific pressure sensor, every 5–20 min depending on the deployment. The Seagauges were modified by adding parallel plate pressure ports to reduce Bernoulli effects associated with blockage of the flow by the instrument housing. To get accurate absolute water depth measurements, small pressure offsets (5–10 cm of water) were corrected by matching the Seagauge pressure measurements to atmospheric pressure for short periods before and after each deployment. Time series of water depth were estimated from the Seagauge near-bottom pressure measurements, assuming hydrostatic flow and using atmospheric pressure measurements near each

site and, for deeper sites, the depth-average density (from Seagauges and SeaBird microCats). Sea levels were estimated relative to the mean water depth at each site and then leveled relative to each other by assuming that the mean sea surface, averaged over times when the current speed was less than  $2 \text{ cm s}^{-1}$ , was flat. Estimated accuracy of sea level difference variations is a few millimeters, based on laboratory tests, intercomparisons, and dynamical balances (e.g., [Lentz et al. 1999](#)).

Bathymetry transects across the Red Sea platform reefs were made using a downward-looking Aquadopp, sampling 2-cm bins, mounted under a float and a Garmin GPS mounted on top of the float. Both sampled at 1 Hz. The estimates of bottom location have a vertical accuracy of about 1 cm and a horizontal resolution of about 0.2 m (based on a float drift velocity of  $0.2 \text{ m s}^{-1}$ ) [see [Lentz et al. \(2016a\)](#) for details]. Bathymetry transects across the Palau and Dongsha reefs were made by a diver towing a Sensus Ultra pressure sensor along the bottom and a Garmin GPS mounted on a surface float ([DeCarlo et al. 2017](#)). The pressure sensor has a resolution of about 1 cm and sampled every 10 s, giving a nominal horizontal resolution of 0.2 m. To distinguish between bathymetry variations and roughness elements, the bathymetry transects were low-pass filtered with a half-power length-scale cutoff of  $L_c = 20 \text{ m}$ . The filter length scale  $L_c$  was based on assuming the scale of the nonlinear advective term ( $U^2/L_c$ ) was the same order as the bottom stress term ( $C_{da}U^2/D$ ). Therefore,  $L_c \approx D/C_{da} \approx 20 \text{ m}$  for  $D \approx 1$  and  $C_{da} \approx 0.05$ . Results are similar if unfiltered bathymetry is used.

For the Red Sea reefs, wind and atmospheric pressure measurements were from a coastal tower on the King Abdullah University of Sciences and Technology (KAUST) campus about 15 km east of Al Fahal reef and 40 km northeast of QD3 reef. For the Palau barrier reef, meteorological measurements were from the Koror Airport approximately 20 km east of the instrument array. At Dongsha, winds were from an anemometer deployed at E5 ([Fig. 5b](#)), with missing wind data from 12 to 17 June filled with the cross-calibrated multiplatform (CCMP) wind product ([Wentz et al. 2015](#)). Wind stresses were estimated following [Fairall et al. \(2003\)](#). Incident surface waves in the Red Sea were measured using a Teledyne RDI ADCP deployed in front of QD2 reef (see [Lentz et al. 2016b](#) for details) and a Seagauge pressure sensor deployed in front of Al Fahal reef. At Dongsha incident surface waves were measured using a Nortek Acoustic Wave and Current (AWAC) meter deployed at E1. There were no measurements of incident surface waves for the Palau barrier reef.

## REFERENCES

- Asher, S., S. Niewerth, K. Koll, and U. Shavit, 2016: Vertical variations of coral reef drag forces. *J. Geophys. Res. Oceans*, **121**, 3549–3563, doi:10.1002/2015JC011428.
- Atkinson, M. J., and R. W. Bilger, 1992: Effects of water velocity on phosphate uptake on coral reefs. *Limnol. Oceanogr.*, **37**, 261–272, doi:10.4319/lo.1992.37.2.0273.
- Baird, M. E., M. Roughan, R. W. Brander, J. H. Middleton, and G. J. Nippard, 2004: Mass-transfer-limited nitrate uptake on a coral reef flat, Warraber Island, Torres Strait, Australia. *Coral Reefs*, **23**, 386–396, doi:10.1007/s00338-004-0404-z.
- Barkley, H. C., A. L. Cohen, Y. Golbuu, V. R. Starczak, T. M. DeCarlo, and K. E. F. Shamberger, 2015: Changes in coral reef communities across a natural gradient in seawater pH. *Sci. Adv.*, **1**, e1500328, doi:10.1126/sciadv.1500328.
- Becker, J. M., M. A. Merrifield, and M. Ford, 2014: Water level effects on breaking wave setup for Pacific Island fringing reefs. *J. Geophys. Res. Oceans*, **119**, 914–932, doi:10.1002/2013JC009373.
- Bernstein, W. N., K. A. Huguen, C. Langdon, D. C. McCorkle, and S. J. Lentz, 2016: Environmental controls on daytime net community calcification on a Red Sea reef flat. *Coral Reefs*, **35**, 697–711, doi:10.1007/s00338-015-1396-6.
- Britter, R. E., and S. R. Hanna, 2003: Flow and dispersion in urban areas. *Annu. Rev. Fluid Mech.*, **35**, 469–496, doi:10.1146/annurev.fluid.35.101101.161147.
- Callaghan, D. P., P. Nielsen, N. Cartwright, M. R. Gourlay, and T. E. Baldock, 2006: Atoll lagoon flushing forced by waves. *Coast. Eng.*, **53**, 691–704, doi:10.1016/j.coastaleng.2006.02.006.
- Coronado, C., J. Candela, R. Iglesias-Prieto, J. Sheinbaum, M. Lopez, and F. J. Ocampo-Torres, 2007: On the circulation in the Puerto Morelos fringing reef lagoon. *Coral Reefs*, **26**, 149–163, doi:10.1007/s00338-006-0175-9.
- DeCarlo, T. M., A. L. Cohen, G. T. F. Wong, F.-K. Shiah, S. J. Lentz, K. A. Davis, K. E. F. Shamberger, and P. Lohmann, 2017: Community production modulates coral reef pH and sensitivity of ecosystem calcification to ocean acidification. *J. Geophys. Res. Oceans*, **122**, 745–761, doi:10.1002/2016JC012326.
- Fairall, C. W., E. F. Bradley, J. E. Hare, A. A. Grachev, and J. B. Edson, 2003: Bulk parameterization of air-sea fluxes: Updates and verification for the COARE Algorithm. *J. Climate*, **16**, 571–591, doi:10.1175/1520-0442(2003)016<0571:BPOASF>2.0.CO;2.
- Feddersen, F., R. T. Guza, S. Elgar, and T. H. C. Herbers, 2000: Velocity moments in alongshore bottom stress parameterizations. *J. Geophys. Res.*, **105**, 8673–8686, doi:10.1029/2000JC900022.
- , E. L. Gallagher, R. T. Guza, and S. Elgar, 2003: The drag coefficient, bottom roughness, and wave-breaking in the nearshore. *Coast. Eng.*, **48**, 189–195, doi:10.1016/S0378-3839(03)00026-7.
- Grant, W. D., and O. S. Madsen, 1986: The continental-shelf bottom boundary layer. *Annu. Rev. Fluid Mech.*, **18**, 265–305, doi:10.1146/annurev.fl.18.010186.001405.
- Hearn, C. J., 1999: Wave-breaking hydrodynamics within coral reef systems and the effect of changing relative sea level. *J. Geophys. Res. Oceans*, **104**, 30007–30019, doi:10.1029/1999JC900262.
- , 2011: Perspectives in coral reef hydrodynamics. *Coral Reefs*, **30**, 1–9, doi:10.1007/s00338-011-0752-4.
- , M. J. Atkinson, and J. L. Falter, 2001: A physical derivation of nutrient-uptake rates in coral reefs: effects of roughness and waves. *Coral Reefs*, **20**, 347–356, doi:10.1007/s00338-001-0185-6.
- Hench, J. L., J. J. Leichter, and S. G. Monismith, 2008: Episodic circulation and exchange in a wave-driven coral reef and lagoon system. *Limnol. Oceanogr.*, **53**, 2681–2694, doi:10.4319/lo.2008.53.6.2681.
- Jago, O. K., P. S. Kench, and R. W. Brander, 2007: Field observations of wave-driven water-level gradients across a coral reef flat. *J. Geophys. Res.*, **112**, C06027, doi:10.1029/2006JC003740.
- Jaramillo, S., and G. Pawlak, 2011: AUV-based bed roughness mapping over a tropical reef. *Coral Reefs*, **30**, 11–23, doi:10.1007/s00338-011-0731-9.
- Jimenez, J., 2004: Turbulent flows over rough walls. *Annu. Rev. Fluid Mech.*, **36**, 173–196, doi:10.1146/annurev.fluid.36.050802.122103.
- Keulegan, G. H., 1938: Laws of turbulent flow in open channels. *J. Res. Natl. Bur. Stand.*, **21**, 707–741, doi:10.6028/jres.021.039.
- Kraines, S. B., T. Yanagi, M. Isobi, and H. Komiyama, 1998: Wind-wave driven circulations on the coral reef at Bora Bay, Miyako Island. *Coral Reefs*, **17**, 133–143, doi:10.1007/s003380050107.
- Lentz, S., R. T. Guza, S. Elgar, F. Feddersen, and T. H. C. Herbers, 1999: Momentum balances on the North Carolina inner shelf. *J. Geophys. Res.*, **104**, 18205–18226, doi:10.1029/1999JC900101.
- , J. H. Churchill, K. A. Davis, J. T. Farrar, J. Pineda, and V. Starczak, 2016a: The characteristics and dynamics of wave-driven flow across a platform coral reef in the Red Sea. *J. Geophys. Res.*, **121**, 1360–1376, doi:10.1002/2015JC011141.
- , —, —, and —, 2016b: Surface gravity wave transformation across a platform coral reef in the Red Sea. *J. Geophys. Res. Oceans*, **121**, 693–705, doi:10.1002/2015JC011142.
- Lowe, R. J., and J. L. Falter, 2015: Oceanic forcing of coral reefs. *Annu. Rev. Mar. Sci.*, **7**, 43–66, doi:10.1146/annurev-marine-010814-015834.
- , —, S. G. Monismith, and M. J. Atkinson, 2009: Wave-driven circulation of a coastal reef-lagoon system. *J. Phys. Oceanogr.*, **39**, 873–893, doi:10.1175/2008JPO3958.1.
- , A. S. Leon, G. Symonds, J. L. Falter, and R. Gruber, 2015: The intertidal hydraulics of tide-dominated reef platforms. *J. Geophys. Res. Oceans*, **120**, 4845–4868, doi:10.1002/2015JC010701.
- Lugo-Fernández, A., H. H. Roberts, and J. N. Suhayda, 1998a: Wave transformations across a Caribbean fringing-barrier coral reef. *Cont. Shelf Res.*, **18**, 1099–1124, doi:10.1016/S0278-4343(97)00020-4.
- , —, and W. J. Wiseman, 1998b: Tide effects on wave attenuation and wave setup on a Caribbean coral reef. *Estuarine Coastal Shelf Sci.*, **47**, 385–393, doi:10.1006/ecss.1998.0365.
- McDonald, C. B., J. R. Koseff, and S. G. Monismith, 2006: Effects of the depth to coral height ratio on drag coefficients for unidirectional flow over coral. *Limnol. Oceanogr.*, **51**, 1294–1301, doi:10.4319/lo.2006.51.3.1294.
- Monismith, S. G., 2007: Hydrodynamics of coral reefs. *Annu. Rev. Fluid Mech.*, **39**, 37–55, doi:10.1146/annurev.fluid.38.050304.092125.
- , L. M. M. Herdman, S. Ahmerkamp, and J. L. Hench, 2013: Wave transformation and wave-driven flow across a steep coral reef. *J. Phys. Oceanogr.*, **43**, 1356–1379, doi:10.1175/JPO-D-12-0164.1.
- , J. S. Rogers, D. Kowek, and R. B. Dunbar, 2015: Frictional wave dissipation on a remarkably rough reef. *Geophys. Res. Lett.*, **42**, 4063–4071, doi:10.1002/2015GL063804.
- Nezu, I., and H. Nakagawa, 1993: *Turbulence in Open-Channel Flows*. A.A. Balkema, 281 pp.
- Nikuradse, J., 1950: Laws of flow in rough pipes. National Advisory Committee for Aeronautics Tech. Memo. 1292, 62 pp. [Available online at <https://ntrs.nasa.gov/search.jsp?R=19930093938>.]



- Nunes, V., and G. Pawlak, 2008: Observations of bed roughness of a coral reef. *J. Coast. Res.*, **24**, 39–50, doi:10.2112/05-0616.1.
- Pomeroy, A., R. Lowe, G. Symonds, A. Van Dongeren, and C. Moore, 2012: The dynamics of infragravity wave transformation over a fringing reef. *J. Geophys. Res.*, **117**, C11022, doi:10.1029/2012JC008310.
- Raubenheimer, R., R. T. Guza, and S. Elgar, 2001: Field observations of wave-driven setdown and setup. *J. Geophys. Res.*, **106**, 4629–4638, doi:10.1029/2000JC000572.
- Raupach, M. R., R. A. Antonia, and S. Rajagopalan, 1991: Rough-wall turbulent boundary layers. *Appl. Mech. Rev.*, **44**, 1–25, doi:10.1115/1.3119492.
- Reidenbach, M. A., S. G. Monismith, J. R. Koseff, G. Yahel, and A. Genin, 2006: Boundary layer turbulence and flow structure over a fringing coral reef. *Limnol. Oceanogr.*, **51**, 1956–1968, doi:10.4319/lo.2006.51.5.1956.
- Roberts, H. H., S. P. Murray, and J. H. Suhayda, 1975: Physical processes in a fringing reef system. *J. Mar. Res.*, **33**, 233–260.
- Rogers, J. S., S. G. Monismith, D. A. Kowalik, W. I. Torres, and R. B. Dunbar, 2016: Thermodynamics and hydrodynamics in an atoll reef system and their influence on coral cover. *Limnol. Oceanogr.*, **61**, 2191–2206, doi:10.1002/lno.10365.
- Rosman, J. H., and J. L. Hench, 2011: A framework for understanding drag parameterizations for coral reefs. *J. Geophys. Res.*, **116**, C08025, doi:10.1029/2010JC006892.
- Rouse, H., 1965: Critical analysis of open-channel resistance. *J. Hydraul. Div.*, **91** (HY4), 1–25.
- Schlichting, H., 1968: *Boundary-Layer Theory*. McGraw-Hill Inc., 747 pp.
- Smart, G. M., M. J. Duncan, and J. M. Walsh, 2002: Relatively rough flow resistance equations. *J. Hydraul. Eng.*, **128**, doi:10.1061/(ASCE)0733-9429(2002)128:6(568).
- Symonds, G., K. P. Black, and I. R. Young, 1995: Wave-driven flow over shallow reefs. *J. Geophys. Res.*, **100**, 2639–2648, doi:10.1029/94JC02736.
- Taebi, S., R. J. Lowe, C. B. Pattiaratchi, G. N. Ivey, G. Symonds, and R. Brinkman, 2011: Nearshore circulation in a tropical fringing reef system. *J. Geophys. Res.*, **116**, C02016, doi:10.1029/2010JC006439.
- Vetter, O., J. M. Becker, M. A. Merrifield, A.-C. Pequignet, J. Aucan, S. J. Boc, and C. E. Pollock, 2010: Wave setup over a Pacific Island fringing reef. *J. Geophys. Res.*, **115**, C12066, doi:10.1029/2010JC006455.
- Wentz, F. J., J. Scott, R. Hoffman, M. Leidner, R. Atlas, and J. Ardizzone, 2015: Remote Sensing Systems Cross-Calibrated Multi-Platform (CCMP) 6-hourly ocean vector wind analysis product on 0.25 deg grid, version 2.0. Remote Sensing Systems, accessed 5 April 2017. [Available online at [www.remss.com/measurements/ccmp](http://www.remss.com/measurements/ccmp).]
- Zawada, B. G., G. A. Piniak, and C. J. Hearn, 2010: Topographic complexity and roughness of a tropical benthic seascape. *Geophys. Res. Lett.*, **37**, L14604, doi:10.1029/2010GL043789.